Molecular Therapy
Nucleic Acids
Original Article

miR-199a-3p Modulates MTOR and PAK4 Pathways and Inhibits Tumor Growth in a Hepatocellular Carcinoma Transgenic Mouse Model

Elisa Callegari,[1] Lucilla D'Abundo,[1] Paola Guerriero,[1] Carolina Simioni,[1] Bahaeldin K. Elamin,[2,3] Marta Russo,[1] Alice Cani,[1] Cristian Bassi,[1] Barbara Zagatti,[1] Luciano Giacomelli,[4] Stella Blandamura,[4] Farzaneh Moshiri,[1,5] Simona Ultimo,[1] Antonio Frassoldati,[1] Giuseppe Altavilla,[4] Laura Gramantieri,[6] Luca Maria Neri,[1] Silvia Sabbioni,[7] and Massimo Negrini[1]

[1]Department of Morphology, Surgery and Experimental Medicine, University of Ferrara, 44121 Ferrara, Italy; [2]Department of Basic Sciences, College of Medicine, University of Bisha, 61922 Bisha, Saudi Arabia; [3]Microbiology Department, Faculty of Medical Laboratory Sciences, University of Khartoum, 11115 Khartoum, Sudan; [4]Department of Medicine DIMED, University of Padova, 35128 Padova, Italy; [5]Department of Molecular Medicine, School of Advanced Technologies in Medicine, Tehran University of Medical Sciences, 11369 Tehran, Iran; [6]Center for Applied Biomedical Research, St. Orsola-Malpighi University Hospital, 40138 Bologna, Italy; [7]Department of Life Sciences and Biotechnology, University of Ferrara, 44121 Ferrara, Italy

Hepatocellular carcinoma (HCC) is the second leading cause of cancer-related death worldwide. Prognosis is poor, and therapeutic options are limited. MicroRNAs (miRNAs) have emerged as potential therapeutic molecules against cancer. Here, we investigated the therapeutic efficacy of miR-199a-3p, an miRNA highly expressed in normal liver and downregulated in virtually all HCCs. The therapeutic value of miR-199a-3p mimic molecules was assayed in the TG221 mouse, a transgenic model highly predisposed to the development of liver cancer. Administration of miR-199a-3p mimics in the TG221 transgenic mouse showing liver cancer led to a significant reduction of number and size of tumor nodules compared to control animals. *In vivo* delivery confirmed protein downregulation of the miR-199a-3p direct targets, mechanistic target of rapamycin (MTOR) and p21 activated kinase 4 (PAK4), ultimately leading to the repression of FOXM1. Remarkably, the anti-tumor activity of miR-199a-3p mimics was comparable to that obtained with sorafenib. These results suggested that miR-199a-3p may be considered a promising HCC therapeutic option.

INTRODUCTION

Hepatocellular carcinoma (HCC) is the second leading cause of cancer-related death worldwide.[1] Despite the development of new therapeutic strategies, prognosis remains poor, and life expectancy after diagnosis of advanced cancer is approximately 6 months.[2] Conventional treatments such as chemotherapy and radiation therapy have limitations, including resistance to treatments and significant toxicity.[3–5] The multi-tyrosine kinase inhibitor sorafenib is the only systemic drug effective in first-line treatments in advanced-stage HCC patients.[6] Very recently, new molecules (regorafenib, lenvatinib, nivolumab, and tremelimumab) have entered or are close to entering clinical use,[7–9] after many failures of clinical trials in the past decade.[10,11] MicroRNAs (miRNAs) have emerged as experimental therapeutic molecules against cancer.[12] miRNAs are small non-coding RNA molecules involved in the post-transcriptional modulation of gene expression, and their aberrant expression is associated with human cancer, including HCC.[13–15]

miR-199a-3p, the third most highly expressed miRNA in normal liver, is downregulated in virtually all HCCs, and its decrement correlates with poor prognosis.[16,17] miRNAs downregulation in liver cancer was associated to phosphorylation of exportin-5 by extracellular signal-related kinase (ERK), a mechanism that decreases export of pre-miRNAs from nucleus.[18] The role of miR-199a-3p in tumorigenesis is still under investigation, but several studies have reported some of its mechanisms of action. It can inhibit cell growth through the downregulation of hypoxia inducible factor 1 alpha subunit (HIFA)[19] and p21 activated kinase 4 (PAK4),[17] and can promote apoptosis through Yes-associated protein 1 (YAP1) inhibition.[20] Restoration of miR-199a-3p in HCC cell lines leads to reduced invasiveness and enhanced doxorubicin sensitivity by controlling the expression of the mechanistic target of rapamycin (*MTOR*), *CD44*, and *MET* proto-oncogene.[21,22] Recently, the ability of miR-199a-3p to suppress tumor growth, migration, invasion, and angiogenesis in HCC by targeting vascular endothelial growth factor A (VEGFA)

Received 12 December 2017; accepted 7 April 2018;
https://doi.org/10.1016/j.omtn.2018.04.002.

Correspondence: Massimo Negrini, PhD, Department of Surgery, Morphology and Experimental Medicine, University of Ferrara, Via Fossato di Mortara 70, 44121 Ferrara, Italy.
E-mail: ngm@unife.it
Correspondence: Elisa Callegari, PhD, Department of Surgery, Morphology and Experimental Medicine, University of Ferrara, Via Fossato di Mortara 70, 44121 Ferrara, Italy.
E-mail: elisa.callegari@unife.it

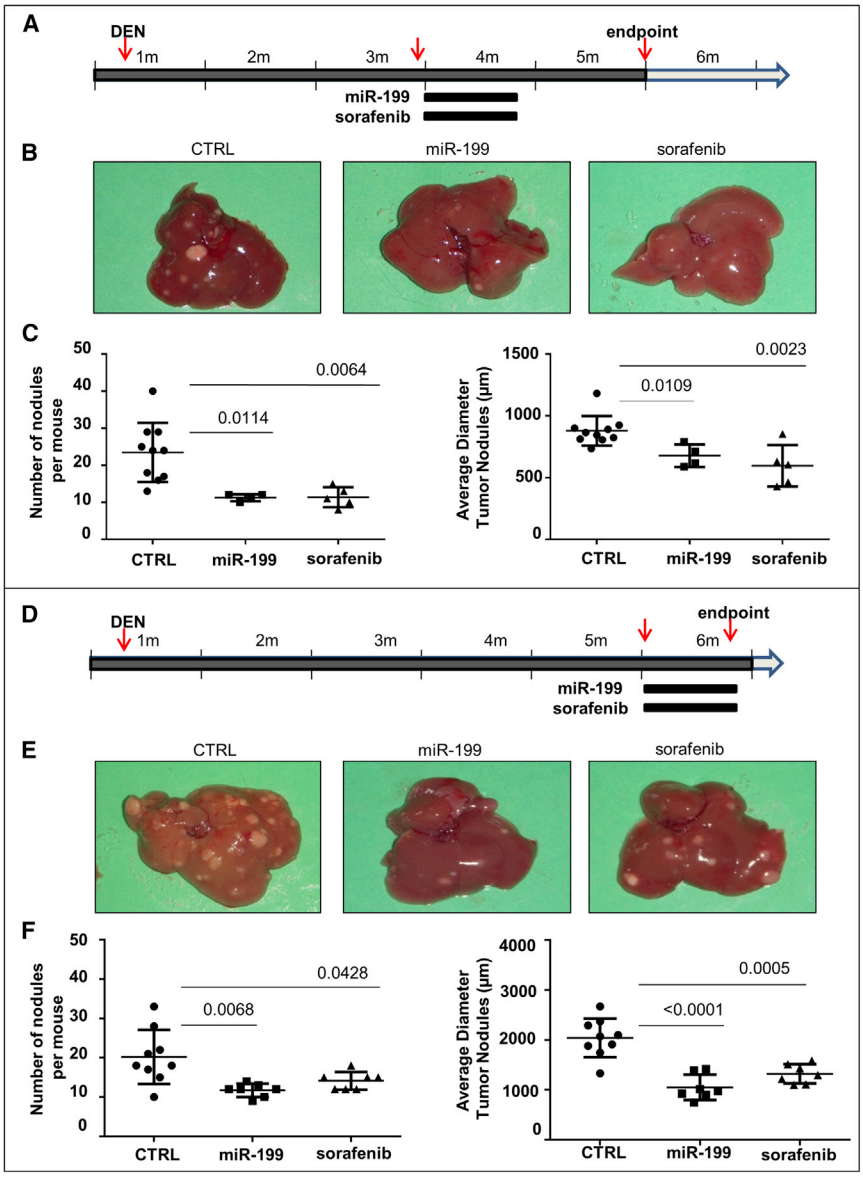

Figure 1. miR-199a-3p Mimics Controlled Liver Tumor Growth

(A) Mice were treated i.p. with the carcinogen *N*-diethylnitrosamine (DEN) at 10 days of age. miR-199a-3p mimics (5 mg/kg) were intraperitoneally injected three times a week for 3 weeks in 3-month-old mice. Identical schedule and amounts of scrambled oligonucleotides were used as negative controls (CTRL). Sorafenib treatment (5 mg/kg, daily oral administration) was used as a positive control for a reference drug in use against liver cancer. (B and C) At 5 months of age, mice were sacrificed, and liver lesions quantified. Number and size of nodules were significantly smaller in mice treated with miR-199a-3p and sorafenib than in the controls. (D) A similar experiment with a larger group of miR-199a-3p-treated mice and a slightly different timing of therapeutic interventions. Treatments began at 5 months of age, and mice were sacrificed immediately after the end of treatment. (E and F) In agreement with the results of the previous experiment, number and size of nodules were significantly smaller in mice treated with miR-199a-3p and sorafenib compared to the controls. In the figure, miR-199a-3p is indicated as miR-199.

and its receptors, hepatocyte growth factor (HGF) and matrix metallopeptidase 2 (MMP2), has been shown.[23]

Here, we investigated the potential therapeutic activity of miR-199a-3p in the TG221 transgenic mouse,[24] a model highly predisposed to the development of liver cancer. Our study shows that miR-199a-3p can produce an anti-tumor effect similar to sorafenib or the MTOR inhibitor WYE-354, by acting on MTOR and PAK4 molecular pathways.

RESULTS

Anti-tumor Activity of miR-199a-3p Was Similar to that of Sorafenib in the TG221 Transgenic Mouse Model

The TG221 transgenic mouse model was employed to assess the therapeutic efficacy of miR-199a-3p. In all experiments, mice were treated intraperitoneally (i.p.) with the carcinogen *N*-diethylnitrosamine (DEN) at 10 days of age to accelerate the appearance of liver tumors. All experiments were performed in male mice.

In the first experiment (Figure 1A), 4 mice (3 months old) received miR-199a-3p mimics (5 mg/Kg) by i.p. injection 3 times a week. Ten mice received scrambled oligonucleotides, and 5 mice received a daily oral administration of sorafenib (5 mg/kg). The i.p. administration was preferred to the intravenous (i.v.) route because the efficiency of miRNA delivery to liver was comparable (Figure S1) and, in case of multiple injections, more feasible and reproducible. All treatments were performed for 3 consecutive weeks. At 5 months old, 1 month after the end of treatments, mice were sacrificed, and number and size of liver lesions were assessed. Multifocal liver lesions were detected, and tumor lesions were either HCCs or dysplastic adenomas as previously described.[24] Detectable tumor nodules were significantly fewer and smaller in miR-199a-3p-treated mice than in control animals (Figures 1B and 1C). Interestingly, the results obtained with miR-199a-3p were comparable to those obtained in mice treated with sorafenib.

In a second independent experiment (Figure 1D), the treatment schedule was slightly modified as it began when the mice were 5 months old and were sacrificed after 3 weeks, 24 hr after the end of the last treatments. Experimental groups were as follows: miR-199a-3p (seven mice), scrambled (nine mice), and sorafenib (seven mice). Measurements of anti-tumor efficacy confirmed the

results of the first experiment. The number and size of nodules were significantly smaller than controls after treatment with miR-199a-3p and comparable with those obtained with sorafenib (Figures 1D–1F). A fourth group of animals (seven mice) was included to assay a possible additive or synergistic anti-tumor effect of the combination miR-199a-3p with sorafenib. The effect was not significantly higher than the single agents (Figure S2A).

Multiple Pathways Were Affected by miR-199a-3p Treatments

To clarify the mechanisms underlying the anti-tumor activity elicited by miR-199a-3p, we collected and analyzed livers immediately after mice sacrifice. We confirmed that liver was the organ most efficiently targeted by miR-199a-3p delivery (Figure S3). miR-199a-3p levels were considerably increased in liver tumors from mice that were injected with miRNA mimics ($p = 0.006$) (Figure 2A). The high level of miR-199a-3p led to a decrease of the target proteins MTOR and PAK4 (Figure 2B). Additionally, proteins of the downstream pathways, including phospho-AKT, phospho-forkhead box O3 (FOXO3), and FOXM1, were also affected (Figure 3). The reduced activity of FOXM1 was also confirmed by the analysis of differentially expressed genes in HCC and normal liver: several genes whose transcription was induced by *Foxm1* were downregulated in miR-199a-3p-treated HCCs to a level that was intermediate between control HCC and normal liver (Figure 3; Table S1). Interestingly, the level of the tumor suppressor phosphatase and tensin homolog (PTEN) protein and mRNA, which was strongly downregulated in tumors (Figure S4), was restored through an indirect mechanism after treatment with miR-199a-3p (Figure 3).

The MTOR Inhibitor WYE-354 Exhibited an Anti-tumor Activity Comparable to that of miR-199a-3p

The importance of MTOR pathway in liver tumors of the TG221 mouse was investigated by evaluating the anti-tumor efficacy of the MTOR inhibitor WYE-354, a specific MTORC1 and MTORC2 inhibitor. Five mice received a daily oral administration of WYE-354 (10 mg/kg) for 3 weeks, five mice received miR-199a-3p mimics as described above, and six mice received scrambled oligonucleotides. At the end of treatments, all mice (6 months old) were sacrificed, and number and size of liver lesions were assessed (Figure 4). Number and size of nodules were reduced in all the groups of treated mice compared to control animals, indicating a similar *in vivo* anti-tumor activity of miR-199a-3p or MTOR inhibitor compound. A fourth group of mice (five animals) received the combinatorial administration of miR-199a-3p and WYE-354. No significant differences were observed between single agents and their combination (Figure S2B). The drug activity was confirmed by the inhibition of phosphorylation at AKT (S-473) and MTOR (S-2481) in mice treated with WYE-354 compared to control animals (Figure S5).

Enforced Expression of miR-199a-3p Induced Apoptosis and Deregulation of the MTOR and PAK4 Signaling Pathways in Human HCC Cells *In Vitro*

To confirm the biological and molecular effects of miR-199a-3p in human cells, we infected the HCC Hep3B and HepG2 cells with an

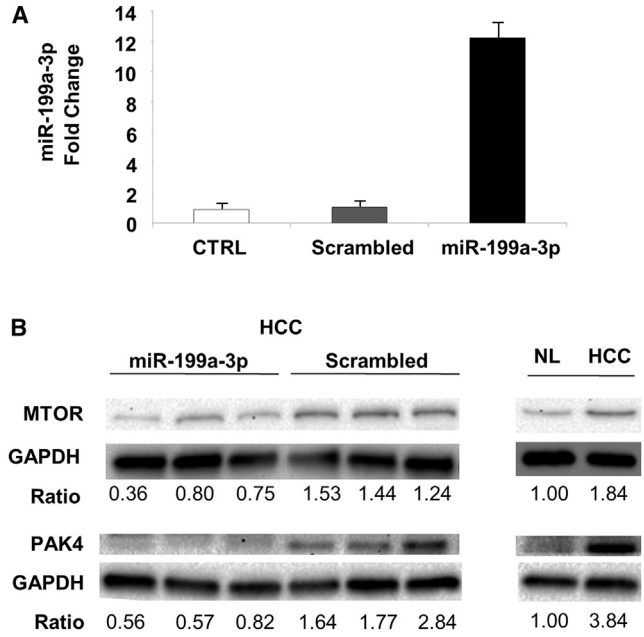

Figure 2. Increased miR-199a-3p Expression Correlated to MTOR Downregulation *In Vivo*

(A) To quantify microRNA (miRNA) molecules at 24 hr from the end of treatments, we performed a droplet digital PCR (ddPCR) on RNA isolated from tumors. A significant increase in miR-199a-3p levels was detected in liver tumors of mice treated with miRNA mimics compared to the other conditions, normal livers (NL), and liver tumors treated with scrambled oligonucleotides ($p = 0.006$). Data are represented as mean + SD. (B) Immunoblotting analysis of hepatocellular carcinoma (HCC) tissues treated with miR-199a-3p revealed downregulation of MTOR and p21 activated kinase 4 (PAK4) proteins compared to the controls. Glyceraldehyde-3-phosphate dehydrogenase (GAPDH) was used as an internal normalizer.

adeno-associated viral vector (AAVV) expressing miR-199a-3p (AAVV-199). The level of miR-199a-3p and its biological effects were evaluated 120 hr post-infection, time needed to allow gene expression from an AAVV. The upregulation of miR-199a-3p caused an increase in cell apoptosis. Weak effects were observed for the control AAVV-GFP (Figure 5). Molecular analyses confirmed the downregulation of MTOR and its phosphorylated form, PAK4, as well as the downregulation of phospho-FOXO3A and FOXM1 proteins (Figure 5). The association between FOXO3A and FOXM1 was confirmed by the enforced overexpression of FOXO3A in Hep3B cells, which induced a decrease in FOXM1 levels compared to the control (Figure S6). The same apoptotic effect was observed in HepG2 cells after miR-199a-3p upregulation (Figure S7).

DISCUSSION

miRNA-based therapies have become of great interest. Restoration of tumor suppressor miRNAs or inhibition of oncogenic miRNAs are approaches that have been used in several pre-clinical models, including liver cancer.[25] The anti-tumor activity of miR-199a-3p has been previously tested in subcutaneous and orthotopic HCC mouse models,[17,19,23,26] confirming the tumor-suppressing activity

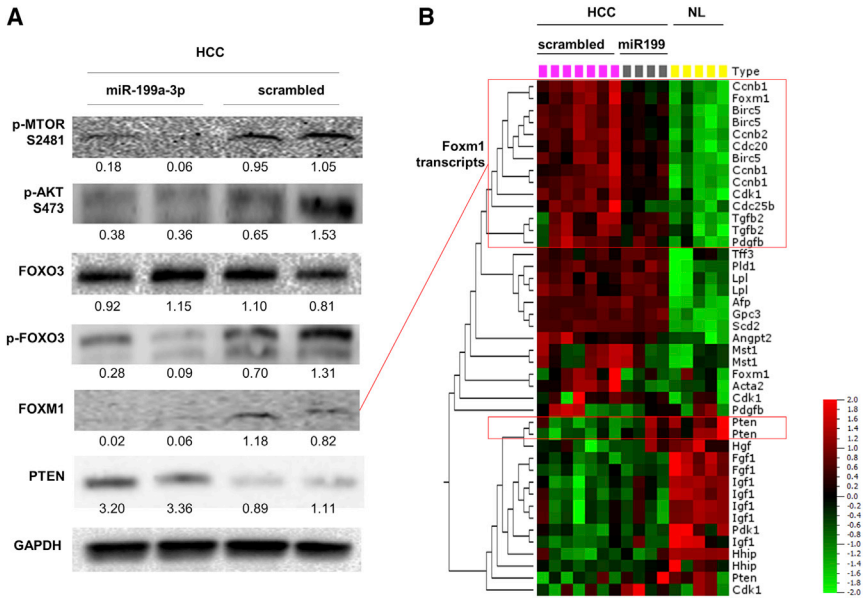

Figure 3. miR-199a-3p Affected MTOR-Associated Pathway *In Vivo*

(A) Immunoblotting analyses of hepatocellular carcinoma (HCC) tissues treated or untreated with miR-199a-3p were performed to investigate the molecular effects of miR-199a-3p on its target genes. We found that proteins involved in the MTOR pathway (phospho-AKT, phospho-forkhead box O3 [pFOXO3], and FOXM1) were downregulated in tumors treated with miR-199a-3p. Phosphatase and tensin homolog (PTEN) protein levels were higher in treated tumors than controls. Glyceraldehyde-3-phosphate dehydrogenase (GAPDH) was used as an internal normalizer. (B) A hierarchical cluster analysis of differentially expressed genes in HCC and normal liver samples (NL) (experiment described in Figure 1D) was performed. Specifically, HCC of scrambled-treated mice, HCC of miR-199a-3p mice, and NL of untreated mice were compared. The analysis showed that several genes controlled by FOXM1 (*Ccnb1*, *Cdc25b*, *Cdc20*, cyclin-dependent kinase 1 [*Cdk1*], transforming growth factor-beta 2 [*Tgfb2*], survivin, and *Foxm1* itself) were downregulated in miR-199a-3p-treated samples. The colors of the genes represent the expression values normalized using the mean expression across all samples (green, downregulated; red, upregulated). (B) miR-199a-3p is indicated as miR-199.

of miR-199a-3p. In the present work, we expanded the evaluation of the anti-tumor activity of miR-199a-3p using the TG221 transgenic mouse.[24] Liver of these mice are characterized by the presence of steatohepatitis, which resembles the human condition named non-alcoholic steatohepatitis (NASH) and develops spontaneous cancers at 9–12 months of age. In this mouse, the treatment with the carcinogen DEN accelerates the appearance of tumors that become visible at 3–4 months of age in all male mice.

We performed various independent experiments to assess the *in vivo* anti-cancer activity of miR-199a-3p in liver tumors of the TG221 mice. Irrespectively of their design, all experiments indicated that miR-199a-3p induced a significant reduction of number and size of tumor nodules, proving the potential usefulness of this miRNA mimic as a therapeutic agent.

As mechanism of action, we have shown that both MTOR and PAK4 oncoproteins are downregulated following miR-199a-3p-enforced expression by *in vivo* mimics delivery into mouse tumors or *in vitro* AAVV infection of human HCC cell lines. Because the importance of these proteins in cancer is well established,[27,28] these data indicate that their downregulation is important for the induction of miR-199a-3p anti-tumor activity.

MTOR is an essential factor of the PI3K-AKT-PTEN molecular pathway, important for cell survival, proliferation, and switch to a glycolytic metabolism. Albeit *MTOR* gene is mutated at lower frequency than other elements of the pathway in human cancer, it is a target of small molecules that are employed as anti-tumor agents in certain cancers of the kidney and breast.

PAK4, which is an effector for small GTPases activated by the HGF receptor MET[29,30] such as RAC or cell division control protein 42 (CDC42), is at the node of various oncogenic pathways.[28,31] PAK4 can activate ERK, AKT, and WNT pathways involved in cell survival and proliferation.[32] PAK4 can also activate signal transducer and activator of transcription 3 (STAT3) and maintain the stem cell phenotype.[33] Finally, PAK4 interacts and phosphorylates several proteins that mediate migration, invasion, angiogenesis, and vascular permeability.[28,29,31] PAK4 mutations and amplification have been reported in human malignancies.[28] Various PAK4 inhibitors have been developed, but none have yet been validated for clinical use.[28]

In the absence of useful PAK4-specific small-molecule inhibitors, we tested the anti-tumor effect of MTOR inhibition by using the drug WYE-354, a second generation inhibitor able to block both MTORC1 and MTORC2[34] in comparison with miR-199a-3p. It has been shown that WYE-354 has anti-tumor activity *in vitro* and *in vivo* in mouse xenografts of human colon, gallbladder, and prostate cancer,[35,36] and is being tested in early-phase trials.[37] In our model, miR-199a-3p and the MTOR inhibitor compound exhibited a comparable anti-tumor activity. These results confirm first the importance of this pathway for tumor development and second the importance of its control for the anti-tumor activity mediated by miR-199a-3p. Interestingly, a strong anti-tumor activity of the WYE-354 inhibitor was previously observed in PTEN null prostatic and glioma cell xenograft models.[35] It is notable that liver tumors of the TG221 model presented a significant PTEN downregulation.

By reducing MTOR and PAK4 functions, miR-199a-3p led to a reduced phosphorylation and degradation of the tumor suppressor

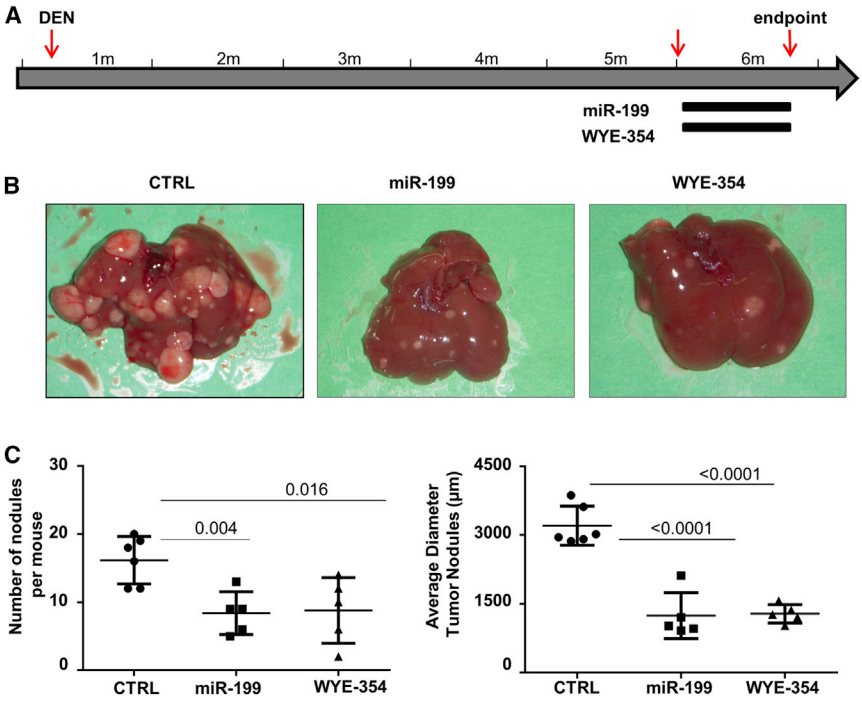

Figure 4. MTOR Inhibitor WYE-354 Had Anti-tumor Activity Comparable to that of miR-199a-3p

(A) The anti-tumor activity of the MTOR inhibitor WYE-354 was tested in TG221 mice. A group of 5-month-old mice, previously treated i.p. with the carcinogen *N*-diethylnitrosamine (DEN) at 10 days of age, received a daily oral administration of WYE-354 (10 mg/kg) for 3 weeks, while a group of mice received miR-199a-3p mimics and scrambled oligonucleotides (CTRL) as scheduled in previous experiments. At the end of treatments, all mice were sacrificed. (B and C) The histological evaluation of liver lesions showed a similar reduction in number and size of tumor nodules in mice treated with both miR-199a-3p and the MTOR inhibitor. In the figure, miR-199a-3p is indicated as miR-199.

protein FOXO3,[38] ultimately leading to the inhibition of the oncogenic FOXM1 transcription factor. An association between FOXO3 and FOXM1 has been previously reported[39,40] and was also confirmed in the present study. The indirect modulation of FOXM1 by miR-199a-3p was confirmed by the analysis of genes whose transcription is controlled by FOXM1: several genes involved in cell-cycle progression, such as *Ccnb1*, *Cdc25b*, *Cdc20*, and cyclin-dependent kinase 1 (*Cdk1*),[41,42] as well as transforming growth factor-beta 2 (*Tgfb2*) and survivin (*Birc5*), were all downregulated in miR-199a-3p-treated samples. The essential role of FOXM1 in hepatic tumor progression has been previously demonstrated *in vivo* by showing its upregulation in DEN-induced liver tumors.[43] Additionally, it has been shown that FOXM1 depletion led to a reduction in the number of tumors in HRas transgenic mice.[44] In humans, *FOXM1* is overexpressed in several solid tumors, including liver,[45] and correlates with poor prognosis of liver cancer patients.[46] Our results indicate that FOXM1 may represent a critical downstream effector of liver tumorigenesis discovered in the TG221 mouse model, and miR-199a-3p exhibits an antitumor action through its inhibition via indirect mechanisms that result from the MTOR and PAK4 controlled pathways.

This study also revealed that miR-199a-3p mimics had an antitumor effect comparable to sorafenib, the only systemic drug currently approved as first line for advanced HCC. Although the therapeutic use of miR-199-3p in place of sorafenib cannot be suggested, it should be noted that miRNA mimics do not show the serious toxicity frequently associated with sorafenib,[47,48] possibly suggesting a testing of miR-199a-3p mimics for patients intolerant to sorafenib. Furthermore, miR-199a-3p was shown to increase susceptibility to doxorubicin-induced apoptosis,[21] suggesting a possible use in combination with other chemotherapeutic agents.

In conclusion, having shown that miR-199a-3p administration led to a reduction of *in vivo* tumor growth comparable to that obtained with sorafenib, and induced growth inhibition and pro-apoptotic activity in human HCC cells, the present study suggests that miR-199a-3p mimics can represent therapeutic molecules potentially useful for the treatment of HCC. In addition, the study highlighted the role of miR-199a-3p in the regulation of MTOR and PAK4 pathways, ultimately leading to inhibition of FOXM1, indicating these oncoproteins as critical effectors of liver cancer and potential direct targets of anti-HCC therapies.

MATERIALS AND METHODS

In Vivo Mouse Studies

The TG221 transgenic mouse was used in all experiments.[24] Mice were maintained in vented cabinets at 25°C with 12-hr light-dark cycle, with food and water *ad libitum*. To facilitate tumor development, 10-day newborn male mice received one i.p. injection of DEN (Sigma-Aldrich, St. Louis, MO, USA) (7.5 mg/kg body weight). The study was performed according with the Guidelines for the Care and Use of Laboratory Animals of the Italian Ministry of Health. To comply with the 2010/63/EU directive of the European Parliament and Council, enforced by the Italian law requiring a minimized number of experimental animals, G*Power (http://www.gpower.hhu.de/) was used to define the sample size for long-term experiments. For short-term experiments, the smallest number of mice sufficient to perform statistical analyses was used. All animals were randomly assigned to different treatment groups at the start of the studies. The protocol for animal experimentation was approved by the Italian Ministry of Health (approval no. 55/2015-PR released on January 29, 2015).

RNA Oligonucleotides for *In Vivo* Therapies

miR-199a-3p and scrambled unmodified single-stranded RNA oligonucleotides were obtained from Axolabs (Kulmbach, Germany).

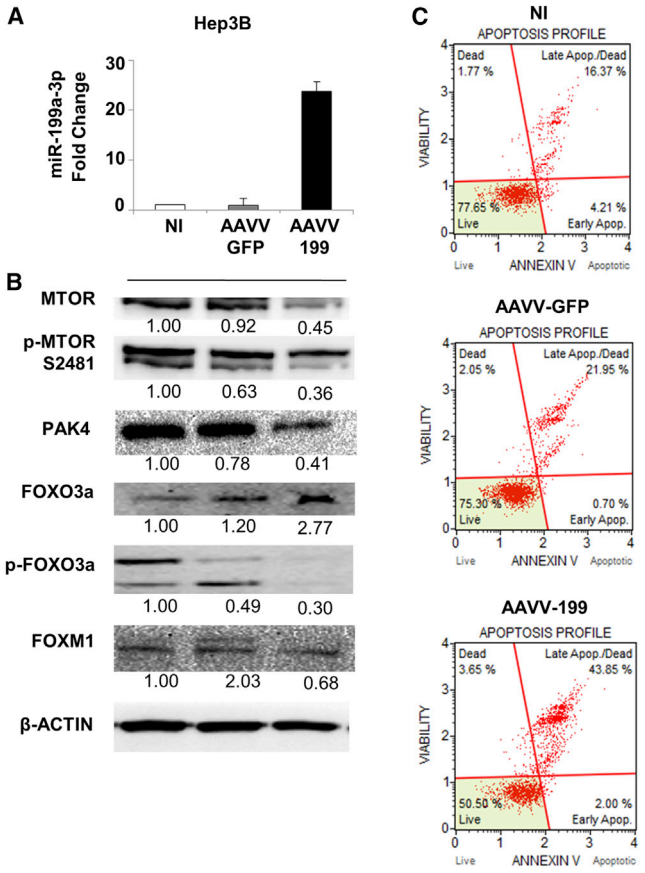

Figure 5. Overexpression of miR-199a-3p Increased Apoptosis Levels in Hep3B Cells by Affecting MTOR and PAK4 Pathways

miR-199a-3p expression increased in Hep3B cells by an adeno-associated viral vector (AAVV) expressing miR-199a-3p (AAVV-199). As experimental controls, the cells were infected with a control virus AAVV- GFP or uninfected. Cells were collected and analyzed 120 hr after infection. (A) The expression levels of miR-199a-3p in the infected cells were determined by qPCR, and proteins were analyzed using immunoblot. miR-199a-3p levels were significantly higher in cells infected with AAVV-199 compared to the controls ($p < 0.0001$). All the data reported are an average of the experiment performed in triplicate (mean + SD). (B) The increased expression of miR-199a-3p-related genes involved in the MTOR and PAK4 pathways. In samples infected with AAVV-199, immunoblotting analyses revealed a downregulation of MTOR and its phosphorylated form p-2481, PAK4, the phosphorylated form of forkhead box O3 (FOXO3a), and FOXM1 compared to the controls (AAVV-GFP, NI). (C) Cells treated with miR-199a-3p showed a considerable increase in the percentage of total apoptosis compared to control cells. Notably, the control virus AAVV-GFP did not induce appreciable changes in cell viability (live cells in the plot) compared to the uninfected control, indicating the non-toxicity of the virus itself and the specificity of the effect mediated by AAVV-199.

In vivo delivery was facilitated by the use of lipid nanoparticles as vehicle. The injections were performed i.p. three times a week for a period of 3 weeks, and oligonucleotides were administered to a final concentration of 5 mg/kg. Mice were randomly enrolled for treatments.

Lipid Nanoparticles

The lipid components of the nanoparticles were 1,2-dioleoyl-sn-glycero-3-phosphoethanolamine (DOPE), 1,2-dimyristoyl-sn-glycerol, methoxypolyethylene glycol (DMG-PEG; Mw 2,000; Avanti Polar Lipids, Alabaster, AL, USA), and linoleic acid (Sigma-Aldrich). The molar ratio of DOPE:linoleic acid:DMG-PEG was 50:48:2. The preparation of empty nanoparticles was performed as previously described.[49]

Anti-tumor Drugs

Sorafenib tosylate (Cat No. S1040; Selleckchem, Houston, TX, USA) was dissolved in a 50:50 Cremophor EL and ethanol solution for *in vivo* experiments. WYE-354 (Cat No. S1266; Selleckchem) was dissolved in dimethyl sulfoxide (DMSO) for *in vitro* experiments and in 4% DMSO, 30% PEG 300, and 5% Tween 80 for *in vivo* experiments as indicated by manufacturer's instructions. The mice received a daily oral administration of sorafenib or WYE-354 at the final concentration of 5 and 10 mg/kg, respectively.

Recombinant AAVV-199

To obtain an AAVV expressing miR-199a-3p, all the plasmids required for AAVV generation (pAAV-IRES-GFP, pAAV-DJ, and pHelper) were purchased from Cell Biolabs (San Diego, CA, USA). The cassette expressing the miR-199a-3p sequence was obtained from the pIRES-miR-199a plasmid[50] and cloned upstream of the IRES-GFP sequence into pAAV-IRES-GFP using *Xba*I sites. The infectious recombinant AAVV-199 was generated by a 1:1:1 (molar ratio) triple transfection of pAAV-199 with helper plasmids (pAAV-DJ and pHelper) into 293FT cells. Viral production and titration were performed as previously reported.[51]

Cell Culture

The HCC cell lines Hep3B (HB-8064) and HepG2 (HB-8065) were obtained from the American Type Culture Collection (ATCC, Manassas, VA, USA). The human embryonic kidney cells 293FT were obtained from Invitrogen (Carlsbad, CA, USA). Cell lines were propagated and maintained in Dulbecco's modified Iscove's medium (IMDM) supplemented with 10% fetal bovine serum (FBS), 0.1% gentamycin, and 1% L-glutamine (Sigma-Aldrich). *In vitro* cell transfections were performed using Lipofectamine 2000 (Invitrogen). A FOXO3 (untagged)-human plasmid (Cat No. SC119227; OriGene Technologies, Rockville, MD, USA) was used for transfection in Hep3B cells.

Apoptosis Assay

The Muse Annexin V and Dead Cell Assay kit (Cat. No. MCH100105; Merck Millipore, Burlington, MA, USA) was used to measure viable, apoptotic, and dead cells in a Muse Cell Analyzer instrument (Cat No. 0500-3115; Merck Millipore). All assays were performed in triplicate.

Western Blot Analyses

Cell cultures were washed with PBS and collected at the defined time point. Tissue samples were collected, immediately frozen in liquid nitrogen, and stored at −80°C until protein extraction. Samples

were dissolved by repeated syringing in radioimmune precipitation (RIPA) buffer (R0278; Sigma-Aldrich) containing phosphatase and protease inhibitors (P2850 and P8340; Sigma-Aldrich). Lysates were centrifuged at 8,000 × *g* for 10 min at 4°C to pellet the debris, and supernatants were collected and analyzed by western blot. Rabbit polyclonal antibodies against PTEN (#9552; Cell Signaling, Danvers, MA, USA), AKT (C6E7, #4691; Cell Signaling), phospho-AKT (Ser473, D9E, #4060; Cell Signaling), MTOR (7C10, #2983; Cell Signaling), phospho-MTOR (Ser2481, #2974; Cell Signaling), FOXO3A (D19A7, #12829; Cell Signaling), phospho-FOXO3A (#2599; Cell Signaling), FOXM1 (TA327372; OriGene Technologies), and PAK4 (#3242; Cell Signaling) were diluted following the manufacturer's instructions and incubated at 4°C for 16 hr. Anti-glyceraldehyde-3-phosphate dehydrogenase (GAPDH) monoclonal antibody (Clone 2D9, TA802519; OriGene Technologies) or anti-β-actin monoclonal antibody (13E5, #4979; Cell Signaling) were used as housekeeping genes. A horseradish-peroxidase-conjugated secondary antibody (#7074; Cell Signaling) was used for chemiluminescent detection. For signal detection, Clarity Western ECL Substrate (Cat No. 170-5060; Bio-Rad, Laboratories, Hercules, CA, USA) was used according to the manufacturer's instructions. Digital images were acquired with Chemidoc (Bio-Rad Laboratories). Signals were quantified by ImageJ software (https://imagej.nih.gov/ij/), and protein expression levels were normalized according to housekeeping protein expression.

Reverse Transcriptase Droplet Digital PCR

Total RNA was extracted from cells and from frozen liver tissues using TRIzol reagent (Invitrogen) according to the manufacturer's instructions. ddPCR was used to measure the expression level of miRNAs. For qPCR analysis, 5 ng of purified RNA was retro-transcribed using TaqMan MicroRNA Reverse Transcription kit (Applied Biosystems, Foster City, CA, USA). cDNA was used for amplification in a 20-μL reaction volume containing ddPCR Supermix for Probes (Bio-Rad Laboratories) and the TaqMan miRNA PCR probe set specific for miR-199a-3p (assay ID002304; Applied Biosystems). Droplets generation, cycling conditions for TaqMan assays, and count of positive droplets were performed as previously described.[52] The relative abundance of miRNAs was normalized using the TaqMan Assays for RNAs U6 (assay ID001973; Applied Biosystems).

Gene Expression

RNAs were hybridized on Agilent Whole Mouse Gene Expression Microarray (G4852A, 8x60K; Agilent Technologies, Palo Alto, CA, USA), and one-color gene expression was performed according to the manufacturer's protocol. Labeled cRNA was synthesized from 100 ng of total RNA using the Low RNA Input Linear Amplification kit (Agilent Technologies) in the presence of cyanine 3-cytosine triphosphate (CTP) (Perkin-Elmer Life Sciences, Boston, MA, USA). Images generated by Agilent scanner and Feature Extraction 10.5 software (Agilent Technologies) were used to obtain the microarray raw data. Qlucore Omics Explorer software (QOE) (https://www.qlucore.com/) (Qlucore AB, Lund, Sweden) was used to analyze microarray data.

Histological Procedures

Tissue samples from at least two representative fragments of each lobe of the liver were taken at autopsy and fixed in 10% phosphate-buffered formalin for 12–24 h and embedded in paraffin. Serial sections were stained with H&E for the histological determination of nodules number and dimension. ImageJ software was used for assessment of nodule sizes.

Statistical Analysis

Statistical significance of group similarity was resolved using a 2-tailed Student's t test. A p value threshold <0.05 was considered significant. When appropriate, group value was expressed in terms of mean ± SD. GraphPad Prism 6.0 (GraphPad Software, La Jolla, CA, USA) was used for data analysis. No samples or animals were excluded from the analyses. None of the investigators were blinded to group allocations.

SUPPLEMENTAL INFORMATION

Supplemental Information includes seven figures and one table and can be found with this article online at https://doi.org/10.1016/j.omtn.2018.04.002.

AUTHOR CONTRIBUTIONS

E.C., S.S., and M.N. conceived and designed research; E.C., L.D.A., P.G., C.S., B.K.E., M.R., A.C., F.M., and S.U. performed the experiments; E.C., L.D.A., S.S., and M.N. analyzed the data; E.C., S.S., and M.N. wrote the manuscript; C.B. and B.Z. performed bioinformatics and statistical analyses; L.G., S.B., and G.A. performed histological analyses; A.F., L.G., and L.M.N. contributed reagents and materials; all authors read and approved the manuscript.

CONFLICTS OF INTEREST

The authors declare no conflicts of interest.

ACKNOWLEDGMENTS

This work was supported by funds from the Italian Association for Cancer Research (AIRC IG grants 15615 and 20055) and the University of Ferrara to M.N. We wish to thank Fernanda Mora and Augusto Bevilacqua for technical and administrative support.

REFERENCES

1. Ferlay, J., Soerjomataram, I., Dikshit, R., Eser, S., Mathers, C., Rebelo, M., Parkin, D.M., Forman, D., and Bray, F. (2015). Cancer incidence and mortality worldwide: sources, methods and major patterns in GLOBOCAN 2012. Int. J. Cancer *136*, E359–E386.

2. Jemal, A., Center, M.M., DeSantis, C., and Ward, E.M. (2010). Global patterns of cancer incidence and mortality rates and trends. Cancer Epidemiol. Biomarkers Prev. *19*, 1893–1907.

3. Vardy, J., Rourke, S., and Tannock, I.F. (2007). Evaluation of cognitive function associated with chemotherapy: a review of published studies and recommendations for future research. J. Clin. Oncol. *25*, 2455–2463.

4. Vardy, J., and Tannock, I. (2007). Cognitive function after chemotherapy in adults with solid tumours. Crit. Rev. Oncol. Hematol. *63*, 183–202.

5. Kim, Y., Joo, K.M., Jin, J., and Nam, D.H. (2009). Cancer stem cells and their mechanism of chemo-radiation resistance. Int. J. Stem Cells *2*, 109–114.

6. Llovet, J.M., Ricci, S., Mazzaferro, V., Hilgard, P., Gane, E., Blanc, J.F., de Oliveira, A.C., Santoro, A., Raoul, J.L., Forner, A., et al.; SHARP Investigators Study Group (2008). Sorafenib in advanced hepatocellular carcinoma. N. Engl. J. Med. *359*, 378–390.

7. Bruix, J., Qin, S., Merle, P., Granito, A., Huang, Y.H., Bodoky, G., Pracht, M., Yokosuka, O., Rosmorduc, O., Breder, V., et al.; RESORCE Investigators (2017). Regorafenib for patients with hepatocellular carcinoma who progressed on sorafenib treatment (RESORCE): a randomised, double-blind, placebo-controlled, phase 3 trial. Lancet *389*, 56–66.

8. Duffy, A.G., Ulahannan, S.V., Makorova-Rusher, O., Rahma, O., Wedemeyer, H., Pratt, D., Davis, J.L., Hughes, M.S., Heller, T., ElGindi, M., et al. (2017). Tremelimumab in combination with ablation in patients with advanced hepatocellular carcinoma. J. Hepatol. *66*, 545–551.

9. Sprinzl, M.F., and Galle, P.R. (2017). Current progress in immunotherapy of hepatocellular carcinoma. J. Hepatol. *66*, 482–484.

10. Llovet, J.M., and Hernandez-Gea, V. (2014). Hepatocellular carcinoma: reasons for phase III failure and novel perspectives on trial design. Clin. Cancer Res. *20*, 2072–2079.

11. Llovet, J.M., Zucman-Rossi, J., Pikarsky, E., Sangro, B., Schwartz, M., Sherman, M., and Gores, G. (2016). Hepatocellular carcinoma. Nat. Rev. Dis. Primers *2*, 16018.

12. Catela Ivkovic, T., Voss, G., Cornella, H., and Ceder, Y. (2017). microRNAs as cancer therapeutics: a step closer to clinical application. Cancer Lett. *407*, 113–122.

13. Calin, G.A., and Croce, C.M. (2006). MicroRNA signatures in human cancers. Nat. Rev. Cancer *6*, 857–866.

14. Negrini, M., Ferracin, M., Sabbioni, S., and Croce, C.M. (2007). MicroRNAs in human cancer: from research to therapy. J. Cell Sci. *120*, 1833–1840.

15. Peng, Y., and Croce, C.M. (2016). The role of microRNAs in human cancer. Signal Transduct. Target. Ther. *1*, 15004.

16. Murakami, Y., Yasuda, T., Saigo, K., Urashima, T., Toyoda, H., Okanoue, T., and Shimotohno, K. (2006). Comprehensive analysis of microRNA expression patterns in hepatocellular carcinoma and non-tumorous tissues. Oncogene *25*, 2537–2545.

17. Hou, J., Lin, L., Zhou, W., Wang, Z., Ding, G., Dong, Q., Qin, L., Wu, X., Zheng, Y., Yang, Y., et al. (2011). Identification of miRNomes in human liver and hepatocellular carcinoma reveals miR-199a/b-3p as therapeutic target for hepatocellular carcinoma. Cancer Cell *19*, 232–243.

18. Sun, H.L., Cui, R., Zhou, J., Teng, K.Y., Hsiao, Y.H., Nakanishi, K., Fassan, M., Luo, Z., Shi, G., Tili, E., et al. (2016). ERK activation globally downregulates miRNAs through phosphorylating exportin-5. Cancer Cell *30*, 723–736.

19. Jia, X.Q., Cheng, H.Q., Qian, X., Bian, C.X., Shi, Z.M., Zhang, J.P., Jiang, B.H., and Feng, Z.Q. (2012). Lentivirus-mediated overexpression of microRNA-199a inhibits cell proliferation of human hepatocellular carcinoma. Cell Biochem. Biophys. *62*, 237–244.

20. Ren, K., Li, T., Zhang, W., Ren, J., Li, Z., and Wu, G. (2016). miR-199a-3p inhibits cell proliferation and induces apoptosis by targeting YAP1, suppressing Jagged1-Notch signaling in human hepatocellular carcinoma. J. Biomed. Sci. *23*, 79.

21. Fornari, F., Milazzo, M., Chieco, P., Negrini, M., Calin, G.A., Grazi, G.L., Pollutri, D., Croce, C.M., Bolondi, L., and Gramantieri, L. (2010). MiR-199a-3p regulates mTOR and c-Met to influence the doxorubicin sensitivity of human hepatocarcinoma cells. Cancer Res. *70*, 5184–5193.

22. Henry, J.C., Park, J.K., Jiang, J., Kim, J.H., Nagorney, D.M., Roberts, L.R., Banerjee, S., and Schmittgen, T.D. (2010). miR-199a-3p targets CD44 and reduces proliferation of CD44 positive hepatocellular carcinoma cell lines. Biochem. Biophys. Res. Commun. *403*, 120–125.

23. Ghosh, A., Dasgupta, D., Ghosh, A., Roychoudhury, S., Kumar, D., Gorain, M., Butti, R., Datta, S., Agarwal, S., Gupta, S., et al. (2017). MiRNA199a-3p suppresses tumor growth, migration, invasion and angiogenesis in hepatocellular carcinoma by targeting VEGFA, VEGFR1, VEGFR2, HGF and MMP2. Cell Death Dis. *8*, e2706.

24. Callegari, E., Elamin, B.K., Giannone, F., Milazzo, M., Altavilla, G., Fornari, F., Giacomelli, L., D'Abundo, L., Ferracin, M., Bassi, C., et al. (2012). Liver tumorigenicity promoted by microRNA-221 in a mouse transgenic model. Hepatology *56*, 1025–1033.

25. Callegari, E., Gramantieri, L., Domenicali, M., D'Abundo, L., Sabbioni, S., and Negrini, M. (2015). MicroRNAs in liver cancer: a model for investigating pathogenesis and novel therapeutic approaches. Cell Death Differ. *22*, 46–57.

26. Guan, J., Liu, Z., Xiao, M., Hao, F., Wang, C., Chen, Y., Lu, Y., and Liang, J. (2017). MicroRNA-199a-3p inhibits tumorigenesis of hepatocellular carcinoma cells by targeting ZHX1/PUMA signal. Am. J. Transl. Res. *9*, 2457–2465.

27. Bhat, M., Sonenberg, N., and Gores, G.J. (2013). The mTOR pathway in hepatic malignancies. Hepatology *58*, 810–818.

28. Radu, M., Semenova, G., Kosoff, R., and Chernoff, J. (2014). PAK signalling during the development and progression of cancer. Nat. Rev. Cancer *14*, 13–25.

29. Paliouras, G.N., Naujokas, M.A., and Park, M. (2009). Pak4, a novel Gab1 binding partner, modulates cell migration and invasion by the Met receptor. Mol. Cell. Biol. *29*, 3018–3032.

30. Aspenström, P., Fransson, A., and Saras, J. (2004). Rho GTPases have diverse effects on the organization of the actin filament system. Biochem. J. *377*, 327–337.

31. Dart, A.E., and Wells, C.M. (2013). P21-activated kinase 4—not just one of the PAK. Eur. J. Cell Biol. *92*, 129–138.

32. Tyagi, N., Bhardwaj, A., Singh, A.P., McClellan, S., Carter, J.E., and Singh, S. (2014). p-21 activated kinase 4 promotes proliferation and survival of pancreatic cancer cells through AKT- and ERK-dependent activation of NF-κB pathway. Oncotarget *5*, 8778–8789.

33. Tyagi, N., Marimuthu, S., Bhardwaj, A., Deshmukh, S.K., Srivastava, S.K., Singh, A.P., McClellan, S., Carter, J.E., and Singh, S. (2016). p-21 activated kinase 4 (PAK4) maintains stem cell-like phenotypes in pancreatic cancer cells through activation of STAT3 signaling. Cancer Lett. *370*, 260–267.

34. Vilar, E., Perez-Garcia, J., and Tabernero, J. (2011). Pushing the envelope in the mTOR pathway: the second generation of inhibitors. Mol. Cancer Ther. *10*, 395–403.

35. Wang, L., Zhu, Y.R., Wang, S., and Zhao, S. (2016). Autophagy inhibition sensitizes WYE-354-induced anti-colon cancer activity in vitro and in vivo. Tumour Biol. *37*, 11743–11752.

36. Weber, H., Leal, P., Stein, S., Kunkel, H., García, P., Bizama, C., Espinoza, J.A., Riquelme, I., Nervi, B., Araya, J.C., et al. (2015). Rapamycin and WYE-354 suppress human gallbladder cancer xenografts in mice. Oncotarget *6*, 31877–31888.

37. Dienstmann, R., Rodon, J., Serra, V., and Tabernero, J. (2014). Picking the point of inhibition: a comparative review of PI3K/AKT/mTOR pathway inhibitors. Mol. Cancer Ther. *13*, 1021–1031.

38. Sarbassov, D.D., Guertin, D.A., Ali, S.M., and Sabatini, D.M. (2005). Phosphorylation and regulation of Akt/PKB by the rictor-mTOR complex. Science *307*, 1098–1101.

39. Nestal de Moraes, G., Bella, L., Zona, S., Burton, M.J., and Lam, E.W. (2016). Insights into a critical role of the FOXO3a-FOXM1 axis in DNA damage response and genotoxic drug resistance. Curr. Drug Targets *17*, 164–177.

40. Zhao, F., and Lam, E.W. (2012). Role of the forkhead transcription factor FOXO-FOXM1 axis in cancer and drug resistance. Front. Med. *6*, 376–380.

41. Laoukili, J., Kooistra, M.R., Brás, A., Kauw, J., Kerkhoven, R.M., Morrison, A., Clevers, H., and Medema, R.H. (2005). FoxM1 is required for execution of the mitotic programme and chromosome stability. Nat. Cell Biol. *7*, 126–136.

42. Wang, X., Kiyokawa, H., Dennewitz, M.B., and Costa, R.H. (2002). The Forkhead Box m1b transcription factor is essential for hepatocyte DNA replication and mitosis during mouse liver regeneration. Proc. Natl. Acad. Sci. USA *99*, 16881–16886.

43. Gusarova, G.A., Wang, I.C., Major, M.L., Kalinichenko, V.V., Ackerson, T., Petrovic, V., and Costa, R.H. (2007). A cell-penetrating ARF peptide inhibitor of FoxM1 in mouse hepatocellular carcinoma treatment. J. Clin. Invest. *117*, 99–111.

44. Kopanja, D., Pandey, A., Kiefer, M., Wang, Z., Chandan, N., Carr, J.R., Franks, R., Yu, D.Y., Guzman, G., Maker, A., and Raychaudhuri, P. (2015). Essential roles of FoxM1 in Ras-induced liver cancer progression and in cancer cells with stem cell features. J. Hepatol. *63*, 429–436.

45. Yu, M., Tang, Z., Meng, F., Tai, M., Zhang, J., Wang, R., Liu, C., and Wu, Q. (2016). Elevated expression of FoxM1 promotes the tumor cell proliferation in hepatocellular carcinoma. Tumour Biol. *37*, 1289–1297.

46. Sun, H., Teng, M., Liu, J., Jin, D., Wu, J., Yan, D., Fan, J., Qin, X., Tang, H., and Peng, Z. (2011). FOXM1 expression predicts the prognosis in hepatocellular carcinoma

patients after orthotopic liver transplantation combined with the Milan criteria. Cancer Lett. *306*, 214–222.

47. Blanchet, B., Billemont, B., Barete, S., Garrigue, H., Cabanes, L., Coriat, R., Francès, C., Knebelmann, B., and Goldwasser, F. (2010). Toxicity of sorafenib: clinical and molecular aspects. Expert Opin. Drug Saf. *9*, 275–287.

48. Lamarca, A., Feliu, J., and Barriuso, J. (2012). Severe toxicity caused by sorafenib in hepatocellular carcinoma match the data from renal cell carcinoma. Br. J. Cancer *106*, 1246.

49. Huang, X., Schwind, S., Yu, B., Santhanam, R., Wang, H., Hoellerbauer, P., Mims, A., Klisovic, R., Walker, A.R., Chan, K.K., et al. (2013). Targeted delivery of microRNA-29b by transferrin-conjugated anionic lipopolyplex nanoparticles: a novel therapeutic strategy in acute myeloid leukemia. Clin. Cancer Res. *19*, 2355–2367.

50. Callegari, E., Elamin, B.K., D'Abundo, L., Falzoni, S., Donvito, G., Moshiri, F., Milazzo, M., Altavilla, G., Giacomelli, L., Fornari, F., et al. (2013). Anti-tumor activity of a miR-199-dependent oncolytic adenovirus. PLoS ONE *8*, e73964.

51. Moshiri, F., Callegari, E., D'Abundo, L., Corrà, F., Lupini, L., Sabbioni, S., and Negrini, M. (2014). Inhibiting the oncogenic mir-221 by microRNA sponge: toward microRNA-based therapeutics for hepatocellular carcinoma. Gastroenterol. Hepatol. Bed Bench *7*, 43–54.

52. Miotto, E., Saccenti, E., Lupini, L., Callegari, E., Negrini, M., and Ferracin, M. (2014). Quantification of circulating miRNAs by droplet digital PCR: comparison of EvaGreen- and TaqMan-based chemistries. Cancer Epidemiol. Biomarkers Prev. *23*, 2638–2642.

OMTN, Volume *11*

Supplemental Information

miR-199a-3p Modulates MTOR and PAK4 Pathways and Inhibits Tumor Growth in a Hepatocellular Carcinoma Transgenic Mouse Model

Elisa Callegari, Lucilla D'Abundo, Paola Guerriero, Carolina Simioni, Bahaeldin K. Elamin, Marta Russo, Alice Cani, Cristian Bassi, Barbara Zagatti, Luciano Giacomelli, Stella Blandamura, Farzaneh Moshiri, Simona Ultimo, Antonio Frassoldati, Giuseppe Altavilla, Laura Gramantieri, Luca Maria Neri, Silvia Sabbioni, and Massimo Negrini

SUPPLEMENTAL FIGURES

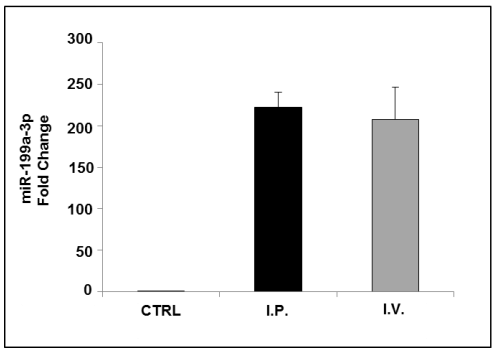

Figure S1. Comparison between intraperitoneal and intravenous systemic administration approaches for *in vivo* miRNA delivery. To find the most efficient and functional route for miRNA administration, intraperitoneal (I.P.) and intravenous (I.V.) injection approaches were compared. Mice received a single dose (2,5mg/kg) of miR-199a-3p by I.P. (n=3) or by I.V. (n=3). Three untreated mice were used as control (CTRL). After 24h, the animals were sacrificed and the levels of miR-199a-3p in livers measured by droplet digital polymerase chain reaction (ddPCR). Results (represented as mean + SD) show that efficacy of the two systemic approaches was comparable.

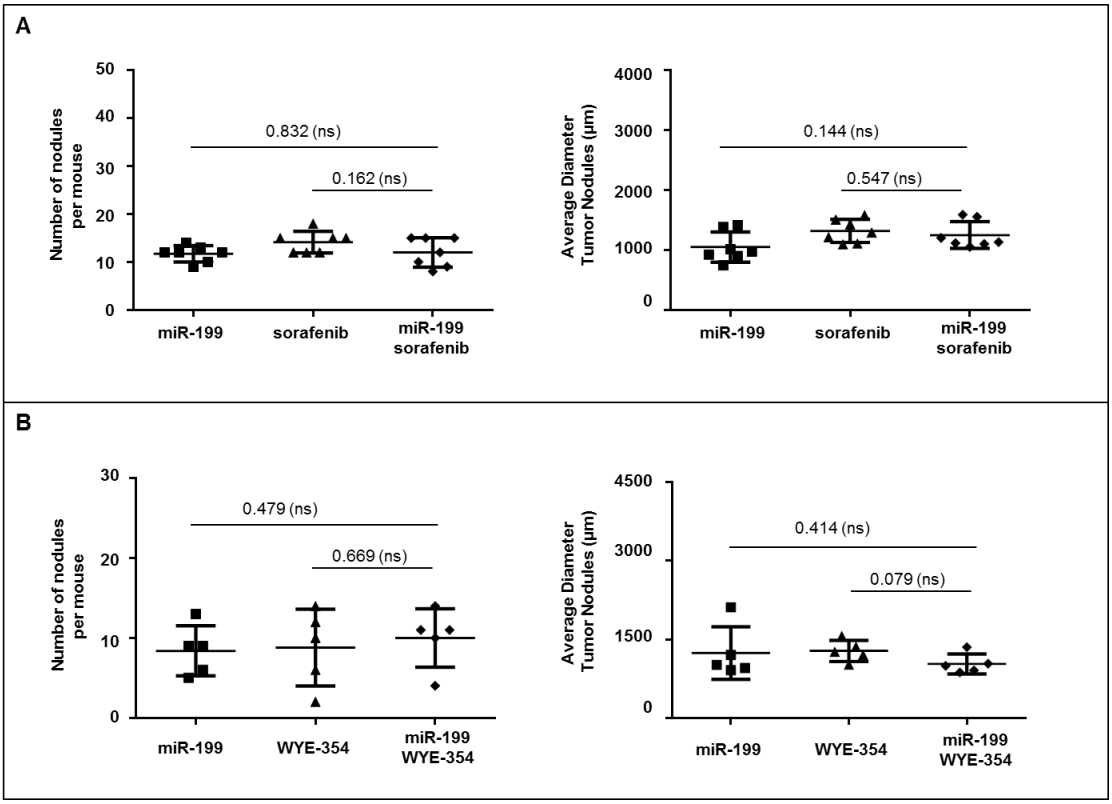

Figure S2. The combination of miR-199a-3p with sorafenib or WYY-354 does not elicit an additive effect. To verify a possible additive anti-tumor effect due to the combination of miR-199a-3p and the tested compounds, additional groups of mice were established. (A) In the context of the experiment described in Figure 1D, 7 mice received a combination of miR-199a-3p and sorafenib. No significant effect on the number and size of nodules was detected. (B) In the context of the experiment described in Figure 4, 5 mice received a combination of miR-199a-3p and WYE-354. No significant differences were observed between single agents and their combination.

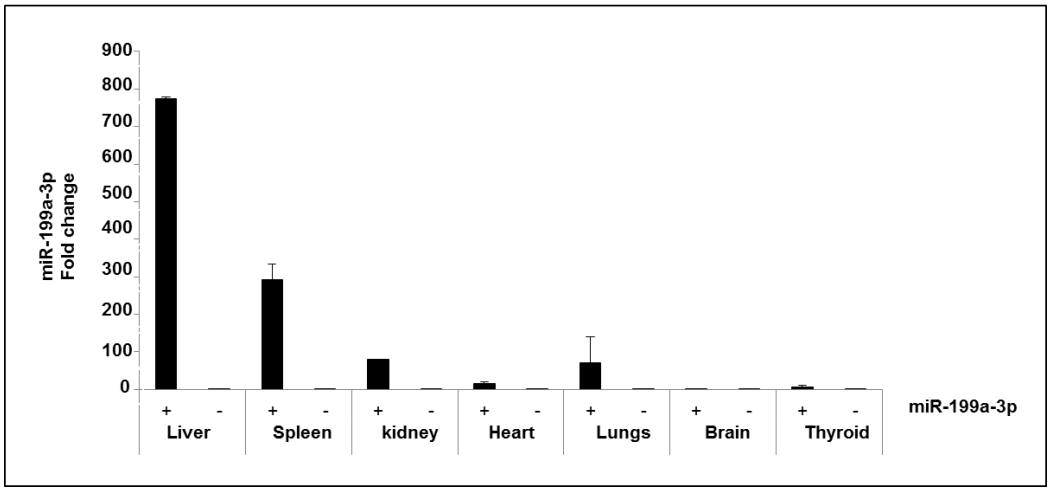

Figure S3. Distribution of miR-199a-3p in various mouse organs following its i.p. administration. To show the delivery of miR-199a-3p molecules *in vivo*, a droplet digital polymerase chain reaction (ddPCR) analysis was performed on several mouse organs. Mice injected with the miRNA (+) were compared with untreated animals (-). All the data represent an average from three animals of each condition (mean + SD)

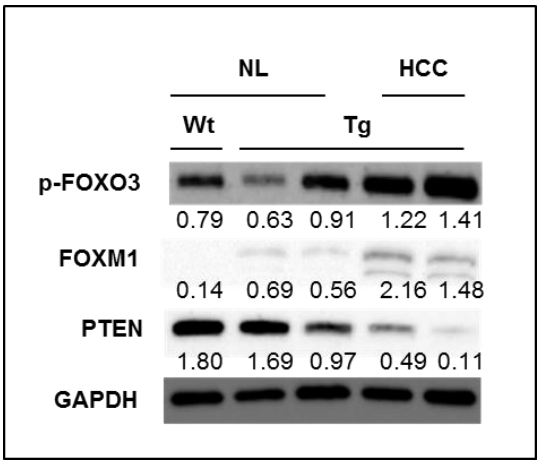

Figure S4. Differential expression of phospho-FOXO3, FOXM1 and PTEN in normal liver and cancer tissues in TG221 mice. Western blot analysis of liver proteins from normal liver of B6D2F2 wild type (wt), TG221 transgenic mice, and liver hepatocellular carcinoma (HCC) from TG221. The analyses showed that HCCs exhibited a higher phosphorylation of FOXO3, upregulation of FOXM1, and downregulation of PTEN compared to normal livers. A slight upregulation of FOXM1 and downregulation of PTEN were observed in normal liver from TG221 mice compared to wt mice. Glyceraldehyde-3-phosphate dehydrogenase (GAPDH) was used as an internal normalizer.

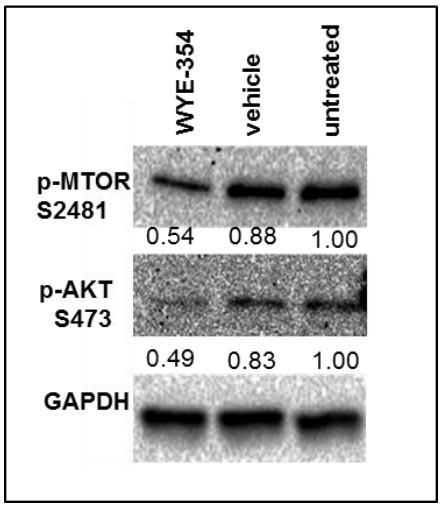

Figure S5. WYE-354 inhibited *in vivo* phosphorylation of AKT and MTOR. Western blot analysis of liver protein extracts from mice treated with WYE-354 and controls. The inhibition of phosphorylation of Akt (S-473) and MTOR (S-2481) was detected in mice treated with WYE-354 compared to control animals. GAPDH was used as an internal normalizer.

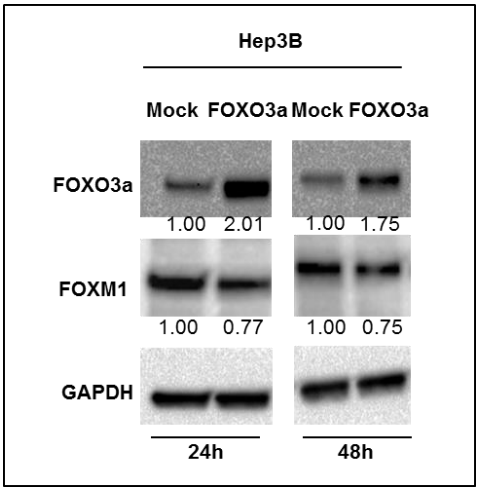

Figure S6. FOXO3A over-expression inhibited FOXM1 expression. Hep3B cells were transfected with a mammalian plasmid vector over-expressing FOXO3a. Cells were collected 24 and 48 h after transfection, and proteins were analyzed by western blot. The over-expression of FOXO3a induced a decrease in FOXM1 levels. Glyceraldehyde-3-phosphate dehydrogenase (GAPDH) was used as an internal normalizer.

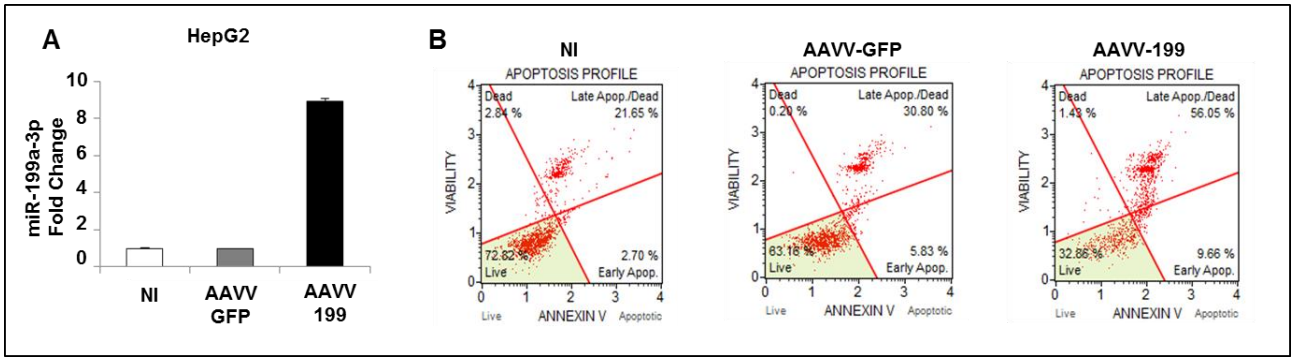

Figure S7. Increased expression of miR-199a-3p enhanced apoptosis levels in HepG2 cells. (A) HepG2 cells were infected with an Adeno Associated Virus (AAVV) expressing miR-199a-3p (AAVV-199). The increase in miR-199a-3p expression levels was detected in the infected cells by quantitative polymerase chain reaction (qPCR). All the data reported are an average of the experiment performed in triplicate. **(B)**. The increased expression of miR-199a-3p caused a statistically significant increase in the percentage of total apoptotic cells compared to the controls ($p < 0.0001$), while AAVV-green fluorescent protein (GFP) effect on cells viability was comparable to the uninfected control (NI)**.** Data are represented as mean + SD.

												Genotype	TG221	TG221	TG221	TG221	TG221	TG221	TG221	TG221	TG221	TG221	TG221	TG221	TG221	TG221	TG221
												Tumor	HCC	HCC	HCC	HCC	HCC	HCC	HCC	HCC	HCC	HCC	HCC	NL	NL	NL	NL	NL
												miR-199a-3p	no	no	no	no	no	no	no	yes	yes	yes	yes	no	no	no	no	no
Gene Symbol	**Agilent ProbeName**	**Foxm1 induced**	**GeneName**	**Organism**	**EntrezGene ID**	**Genbank Accession**	**Average HCC**	**Average HCC + miR-199**	**Average Normal Liver**	**p-value**	**q-value**																		
Acta2	A_52_P420504	no	actin, alpha 2, smooth muscle, aorta	Mus musculus	11475	NM_007392	4.33	0.95	1.00	4.97E-04	9.29E-04		1.95	1.87	3.10	5.07	5.01	10.13	3.20	1.03	1.34	0.76	0.67	1.09	1.49	1.10	0.90	0.39
Afp	A_51_P510891	no	alpha fetoprotein	Mus musculus	11576	NM_007423	245.05	355.63	1.03	8.74E-10	1.25E-08		216.47	182.68	170.58	191.27	259.32	307.34	387.67	780.58	186.88	223.34	231.71	3.29	0.58	0.47	0.35	0.44
Angpt2	A_51_P201982	no	angiopoietin 2	Mus musculus	11601	NM_007426	0.61	0.39	0.17	1.03E-03	1.70E-03		0.88	0.66	1.07	0.48	0.34	0.45	0.39	0.42	0.38	0.48	0.28	0.23	0.06	0.22	0.23	0.13
Birc5	A_55_P1983773	yes	baculoviral IAP repeat-containing 5	Mus musculus	11799	NM_001012273	19.32	7.55	1.37	4.91E-07	4.23E-06		15.67	12.09	13.45	28.30	18.65	34.21	12.86	5.70	8.50	6.00	10.00	0.90	0.62	3.00	1.36	0.99
Birc5	A_55_P1983768	yes	baculoviral IAP repeat-containing 5	Mus musculus	11799	NM_009689	1.66	0.51	0.10	1.15E-06	6.19E-06		1.36	1.00	1.18	2.56	1.55	3.00	0.95	0.55	0.61	0.39	0.50	0.07	0.03	0.26	0.08	0.07
Birc5	A_55_P1983769	yes	baculoviral IAP repeat-containing 5	Mus musculus	11799	NM_001012273	0.51	0.20	0.04	1.33E-05	4.08E-05		0.43	0.27	0.17	0.61	0.65	1.16	0.29	0.17	0.20	0.17	0.26	0.04	0.04	0.08	0.05	0.02
Ccnb1	A_55_P1952256	yes	cyclin B1	Mus musculus	268697	NM_172301	0.41	0.10	0.03	1.08E-06	6.19E-06		0.21	0.34	0.28	0.54	0.43	0.83	0.24	0.10	0.13	0.08	0.10	0.03	0.03	0.07	0.02	0.02
Ccnb1	A_55_P2128668	yes	cyclin B1	Mus musculus	268697	NM_172301	0.43	0.24	0.05	6.24E-06	2.98E-05		0.21	0.23	0.28	0.32	0.45	1.01	0.49	0.19	0.26	0.17	0.35	0.04	0.04	0.08	0.03	0.04
Ccnb1	A_55_P2065671	yes	cyclin B1	Mus musculus	268697	NM_172301	4.13	1.68	0.22	1.59E-07	1.71E-06		2.25	2.60	3.88	3.24	3.91	8.93	4.08	1.51	1.59	1.47	2.15	0.16	0.26	0.42	0.09	0.16
Ccnb2	A_51_P457528	yes	cyclin B2	Mus musculus	12442	NM_007630	9.33	3.14	0.74	1.05E-06	6.19E-06		6.05	6.61	4.52	13.94	8.08	17.88	8.27	3.00	3.99	2.22	3.33	0.53	0.47	1.50	0.45	0.77
Cdc20	A_55_P1996946	yes	cell division cycle 20 homolog (S. cerevisiae)	Mus musculus	107995	NM_023223	8.99	4.42	0.70	1.34E-05	4.08E-05		3.75	7.21	4.08	9.94	10.21	20.43	7.34	3.30	5.53	3.55	5.29	0.38	0.22	1.93	0.47	0.49
Cdc25b	A_52_P612382	yes	cell division cycle 25 homolog B (S. pombe)	Mus musculus	12531	NM_023117	0.83	0.24	0.14	3.79E-05	9.59E-05		0.37	0.79	0.59	0.69	0.76	2.00	0.61	0.27	0.32	0.17	0.18	0.12	0.08	0.19	0.15	0.17
Cdk1	A_55_P2048588	yes	cyclin-dependent kinase 1	Mus musculus	12534	NM_007659	0.68	0.27	0.06	1.42E-05	4.08E-05		0.73	0.44	0.69	0.49	0.86	1.25	0.31	0.25	0.23	0.29	0.31	0.03	0.03	0.19	0.04	0.02
Fgf1	A_55_P2047188	no	fibroblast growth factor 1	Mus musculus	14164	NM_010197	12.64	12.35	32.85	1.03E-05	3.68E-05		15.78	12.66	16.03	10.01	11.39	8.60	13.98	12.25	12.68	13.35	11.11	23.57	35.39	34.19	45.89	25.21
Fgf1	A_52_P538673	no	fibroblast growth factor 1	Mus musculus	14164	NM_010197	0.38	0.39	1.19	8.82E-06	3.61E-05		0.40	0.34	0.46	0.24	0.32	0.54	0.38	0.30	0.43	0.44	0.40	0.88	1.18	1.33	1.73	0.85
Foxm1	A_52_P28806		forkhead box M1	Mus musculus	14235	NM_008021	1.29	0.59	0.21	6.30E-05	1.50E-04		0.62	1.04	0.80	1.36	1.65	2.72	0.85	0.63	0.70	0.36	0.67	0.20	0.17	0.42	0.14	0.12
Gpc3	A_52_P23225	no	glypican 3	Mus musculus	14734	NM_016697	25.44	45.63	0.10	2.75E-10	5.92E-09		22.08	18.49	28.39	23.74	21.82	19.82	43.72	46.36	21.00	34.88	80.28	0.04	0.04	0.28	0.08	0.05
Hgf	A_51_P484998	no	hepatocyte growth factor	Mus musculus	15234	NM_010427	0.28	0.50	0.80	1.75E-02	2.15E-02		0.34	0.35	0.52	0.23	0.08	0.26	0.17	0.26	0.27	0.97	0.52	1.42	0.49	0.84	0.73	0.50
Hhip	A_55_P1969276	no	Hedgehog-interacting protein	Mus musculus	15245	NM_020259	0.08	0.12	0.80	3.64E-04	7.11E-04		0.34	0.06	0.02	0.02	0.01	0.05	0.07	0.12	0.03	0.04	0.28	0.79	0.68	0.80	0.99	0.77
Igf1	A_55_P2085979	no	insulin-like growth factor 1	Mus musculus	16000	NM_184052	2.56	3.70	10.38	2.80E-03	4.01E-03		2.76	1.86	2.45	2.08	2.23	3.92	2.59	2.84	6.99	2.47	2.52	13.50	4.47	14.14	16.30	3.50
Igf1	A_55_P2085974	no	insulin-like growth factor 1	Mus musculus	16000	NM_010512	4.05	4.94	24.32	3.31E-04	6.78E-04		10.85	2.69	3.10	1.08	4.12	4.35	2.15	2.62	9.78	5.50	1.87	23.50	13.90	30.35	32.16	21.71
Igf1	A_55_P2031636	no	insulin-like growth factor 1	Mus musculus	16000	NM_010512	0.80	1.48	6.22	7.67E-05	1.74E-04		1.58	0.40	0.57	0.18	0.87	1.34	0.68	0.87	2.77	1.45	0.83	7.09	4.68	6.36	7.70	5.25
Igf1	A_55_P2085984	no	insulin-like growth factor 1	Mus musculus	16000	NM_010512	29.40	28.88	121.85	3.10E-03	4.31E-03		74.28	14.06	22.65	4.36	27.08	43.27	20.10	21.91	62.90	21.88	8.84	152.64	130.41	103.22	99.98	122.99
Igf1	A_55_P2031631	no	insulin-like growth factor 1	Mus musculus	16000	NM_010512	38.71	40.60	164.58	3.21E-03	4.32E-03		95.71	18.11	28.94	5.74	34.78	59.49	28.21	30.03	88.05	31.40	12.92	214.55	183.57	132.87	126.17	165.72
Lpl	A_52_P257812	no	lipoprotein lipase	Mus musculus	16956	NM_008509	9.52	10.96	1.70	8.67E-05	1.86E-04		13.40	8.97	12.45	5.18	14.34	7.30	4.99	14.14	11.46	10.07	8.17	3.32	1.61	0.66	0.46	2.44
Lpl	A_51_P259296	no	lipoprotein lipase	Mus musculus	16956	NM_008509	67.82	69.95	7.67	9.23E-06	3.61E-05		117.19	78.17	96.15	48.12	66.73	36.53	31.82	71.07	70.00	91.13	47.62	14.34	6.04	3.46	2.82	11.71
Mst1	A_55_P1984098	no	macrophage stimulating 1 (hepatocyte growth factor-like)	Mus musculus	15235	NM_008243	108.66	100.01	79.97	4.43E-02	5.14E-02		125.37	100.99	85.13	84.00	113.43	132.32	119.40	131.02	104.71	80.82	83.48	87.63	90.70	66.89	68.60	86.03
Mst1	A_55_P2115392	no	macrophage stimulating 1 (hepatocyte growth factor-like)	Mus musculus	15235	NM_008243	99.08	91.21	71.96	3.65E-02	4.35E-02		109.24	90.69	77.19	77.47	105.64	121.65	111.69	117.58	96.26	75.00	75.99	82.33	81.17	58.72	59.84	77.73
Pdgfb	A_55_P2047310	yes	platelet derived growth factor, B polypeptide	Mus musculus	18591	NM_011057	1.58	1.22	0.58	7.56E-04	1.35E-03		0.76	1.75	2.41	1.74	1.53	1.23	1.60	0.93	1.65	1.36	0.96	0.54	0.40	0.99	0.53	0.45
Pdk1	A_51_P406429	no	pyruvate dehydrogenase kinase, isoenzyme 1	Mus musculus	228026	NM_172665	1.61	1.51	6.44	2.57E-03	3.82E-03		2.54	1.57	1.88	1.05	1.10	2.27	0.84	1.29	1.93	1.31	1.50	3.57	1.67	10.69	10.24	6.03
Pld1	A_55_P2104487	no	phospholipase D1	Mus musculus	18805	NM_001164056	5.06	5.63	1.45	1.70E-05	4.58E-05		4.91	4.62	5.69	6.61	4.25	4.70	4.64	5.33	4.04	7.40	5.74	1.75	1.98	0.91	0.60	1.99
Pten	A_52_P24843	no	phosphatase and tensin homolog	Mus musculus	19211	NM_008960	1.83	2.23	2.70	1.29E-02	1.64E-02		2.45	1.64	1.82	1.52	1.76	1.62	1.97	1.76	1.92	2.95	2.30	2.62	2.39	2.09	2.91	3.48
Pten	A_51_P275350	no	phosphatase and tensin homolog	Mus musculus	19211	NM_008960	19.58	24.09	27.57	8.68E-04	1.49E-03		20.10	16.96	20.50	20.68	18.37	18.43	22.05	22.98	21.45	28.38	23.56	28.72	28.50	22.39	25.33	32.94
Scd2	A_51_P129464	no	stearoyl-Coenzyme A desaturase 2	Mus musculus	20250	NM_009128	120.54	102.19	1.08	4.08E-12	1.76E-10		104.39	97.13	82.64	166.15	150.83	118.63	124.03	118.50	80.01	112.39	97.88	0.81	0.48	1.65	1.30	1.14
Tff3	A_51_P456208	no	trefoil factor 3, intestinal	Mus musculus	21786	NM_011575	609.00	1010.38	124.46	9.13E-03	1.19E-02		898.70	451.82	795.32	133.85	681.09	272.54	1029.69	1284.51	1287.18	697.91	771.92	226.44	329.86	0.97	0.51	64.50
Tgfb2	A_65_P10913	yes	transforming growth factor, beta 2	Mus musculus	21808	NM_009367	1.07	0.68	0.18	1.07E-03	1.70E-03		0.20	0.96	1.61	0.65	0.56	1.73	1.77	0.51	0.67	0.73	0.83	0.11	0.16	0.33	0.18	0.12
Tgfb2	A_51_P317640	yes	transforming growth factor, beta 2	Mus musculus	21808	NM_009367	0.35	0.23	0.07	2.12E-03	3.25E-03		0.10	0.39	0.58	0.22	0.22	0.43	0.52	0.14	0.22	0.33	0.25	0.03	0.06	0.15	0.11	0.03

Table S1. Expression data of genes from Figure 3